

# T-matrix approach for calculating local fields around clusters of rotated spheroids

William Vargas, Luis Cruz, Luis F. Fonseca, and Manuel Gómez

A T-matrix formalism is used to calculate local electric fields around clusters of prolate spheroids in the long-wavelength regime. The calculations are performed as a function of interparticle distance as well as angle of orientation. The observed red shifts in the resonant wavelengths of the characteristic peaks are shown to obey an exponential relationship as a function of interparticle separation and a sinusoidal relationship as a function of angle of rotation of the spheroid. The behavior of the cluster is discussed and the two effects of separation and rotation are compared.

## 1. Introduction

Optical properties of systems of particles whose size is smaller than the wavelength of the incident electromagnetic radiation have been studied for a long time,<sup>1,2</sup> but the effect of the clustering of such particles is not yet well understood. Recent interest has developed in this subject because clustering is essential to the understanding of many physical processes of interest. Moreover, the current calculations of local scattered electric fields are directly applicable to fields such as surface-enhanced Raman scattering and light scattering and absorption from metallic colloids in alkali halide crystals.<sup>3-8</sup>

Clusters of spheres have been analyzed, primarily in the radiation zone<sup>9-12</sup> or with the use of an electrostatic approach.<sup>10,13</sup> The purpose of this study is to calculate the local electrodynamic field around clusters of two prolate spheroids in the long-wavelength regime as a function of the separation between them and of their relative orientations by using a T-matrix approach, which describes electromagnetic scattering for a general wave that is incident on objects of arbitrary shape. Although the formalism can be used to calculate important parameters in the radiative regime, such as scattering cross sections, the local fields are the major concern here.

The T-matrix method permits an electrodynamic

approach that considers vectorial multipolar fields, in contrast to other recent electrostatic approaches that consider scalar multipolar potentials.<sup>10</sup> The extension to two scatterers is achieved by using an effective T matrix for more than one scatterer, which retains all the advantages of the T matrix for the single scatterer and also permits calculations for scatterers made up of clusters of metallic particles of arbitrary shape. The rotation of the individual T matrices corresponding to any given particle is achieved by using a transformation of the spherical harmonics under finite rotations. This study extends previous research on the calculations of the scattered electric field in the vicinity of clusters of metallic scatterers.<sup>14</sup> In this vicinity two-particle clusters of various configurations gave enhancements of up to  $10^3$  and demonstrated the existence of a critical distance greater than the touching distance between the scatterers at which maximum enhancement was obtained.

We demonstrate that because of clustering interactions the calculated spectrum shows two peaks for the case of clusters of two small prolate spheroids aligned in the direction of the incident electric field, in contrast to the spectrum of the isolated small prolate spheroid that has only one peak. The principal peak decreases in intensity and shifts exponentially as a function of interparticle distance to the value of the resonance for the isolated spheroid, whereas the secondary peak has a vanishing intensity that decreases exponentially as a function of interparticle distance. A decoupling interparticle distance  $d$  of  $4b$ , where  $b$  is the semimajor axis of the prolate spheroids that make up the cluster, is observed. At that distance the behavior of the cluster near any one of the two constituent particles equals that of one

---

W. Vargas is with the Escuela de Física, Universidad de Costa Rica, San Jose, Costa Rica. The other authors are with the Department of Physics, University of Puerto Rico, Rio Piedras, Puerto Rico 00931.

Received 13 August 1991.

0003-6935/93/122164-07\$05.00/0.

© 1993 Optical Society of America.

isolated spheroid. It is shown that there is also a shift in wavelength to the red as a result of the rotation of the spheroids and that this shift varies sinusoidally as a function of orientation.

For all the calculations herein, silver was taken as a model metal by using the complex frequency-dependent dielectric function reported in the literature for the bulk material,<sup>15</sup> although the method is applicable to any material for which the complex dielectric constant is known. For the range of sizes used in these calculations, an electronic mean free path reduced by the boundary of the scatterer or quantum size effects could introduce some modifications to the data for silver used here.

Section 2 presents the T-matrix formalism developed for isolated particles and its modification for metallic clusters. The calculations are done as expansions in vector spherical harmonics  $\Psi_n$ , whose number  $n$  corresponds to terms in the multipolar expansion of the electromagnetic field. Because our main objective is to study clusters, spherical harmonics are used as a convenient basis. A rotation of the T matrix corresponding to a single scatterer is performed, permitting consideration of geometries where the spheroids in the cluster have arbitrary relative orientations.

Section 3 presents the calculation of the local electric fields for these clusters. The clusters are analyzed as a function of separation between spheroids and as a function of angle of orientation with respect to the incident wave. The rate of change of the wavelength shift as a function of interparticle distance and angle of orientation is then discussed. In Section 4 conclusions are presented.

## 2. Formalism

### A. Single Scatterers

The T-matrix formalism developed by Waterman<sup>16</sup> takes into account multipolar contributions, which are essential for any valid calculation of local fields of single nonspherical particles as well as for all clusters even when they are in the long-wavelength regime. The formalism also takes into account phase-retardation effects caused by the size of the scatterers, which are important for particles and clusters whose sizes are comparable with the wavelength of the incident field.

In this method the scattered, internal, and incident fields are expanded in terms of the corresponding elementary fields that are a basis set of solutions for the vector Helmholtz equation,

$$\nabla \times \nabla \times \Psi - k^2 \Psi = 0. \quad (1)$$

The incident  $\epsilon_0$  and internal  $\epsilon_i$  fields are expanded in terms of the basis that is regular at the origin  $\text{Re } \Psi$  and the scattered  $\epsilon_s$  field in terms of the nonregular  $\Psi$

one,

$$\begin{aligned} \epsilon_0 &= \sum_n A_n \text{Re } \Psi_n, \\ \epsilon_i &= \sum_n D_n \text{Re } \Psi_n, \quad |\mathbf{r}| < r_{\min}, \\ \epsilon_s &= \sum_n F_n \Psi_n, \quad |\mathbf{r}| > r_{\max}, \end{aligned} \quad (2)$$

where  $A_n$  are known coefficients,  $D_n$  and  $F_n$  are unknown,  $r_{\min}$  is the radius of the maximum sphere inscribed in the scatterer, and  $r_{\max}$  is the minimum sphere inscribing the scatterer.

The elementary wave functions are expressed as

$$\Psi_{\tau\sigma mn}(\mathbf{r}) = \gamma_{mn}^{1/2} (k^{-1} \nabla \times)^{\tau} [k \mathbf{r} y_{\sigma mn}(\hat{r}) h_n(kr)], \quad (3)$$

where  $\tau = 1, 2$ ,  $\sigma = \text{even}(e)$  or  $\text{odd}(o)$ ,  $n = 1, 2, \dots$ ,  $m = 0, 1, \dots, n$ ,

$$\gamma_{mn} = \epsilon_m \frac{(2n+1)(n-m)!}{4n(n+1)(n+m)!},$$

$$Y_{emn}(\hat{r}) = \cos(m\phi) P_n^m(\cos \theta),$$

$$Y_{omn}(\hat{r}) = \sin(m\phi) P_n^m(\cos \theta).$$

The index  $\tau = 1, 2$  describes the type of excitation, magnetic or electric;  $\epsilon_m$  is the Neumann symbol defined as  $\epsilon_0 = 1$  and  $\epsilon_m = 2$  otherwise;  $n$  is the order of the multipole; and  $\sigma$  gives the parity of the elementary functions. The regular form of the basis functions are obtained by substituting the Hankel functions with the Bessel functions.

The surface currents on the scatterers are used to express the expansion coefficients of the internal field with those of the scattered and incident fields, respectively, by the following relationships:

$$\mathbf{F} = -i \text{Re}(\underline{\mathbf{Q}}') \mathbf{G}, \quad (4)$$

$$\mathbf{A} = i \underline{\mathbf{Q}}' \mathbf{G}, \quad (5)$$

where  $\mathbf{G}$  represents the vector of the expansion coefficients of the internal field and  $\underline{\mathbf{Q}}'$  represents the transpose of the  $\underline{\mathbf{Q}}$  matrix. For a particle with a complex dielectric function,  $\underline{\mathbf{Q}}$  is given by

$$\begin{aligned} Q_{nn'} &= \frac{k_0}{\pi} \int_s ds \{ [\nabla \times \text{Re } \Psi_n(k\mathbf{r})] \times \Psi_{n'}(k_0\mathbf{r}) \\ &\quad + \text{Re } \Psi_n(k\mathbf{r}) \times [\nabla \times \Psi_{n'}(k_0\mathbf{r})] \}, \end{aligned} \quad (6)$$

where  $k_0^2 = \epsilon_{\text{ext}} \omega^2 / c^2$  and  $k^2 = \epsilon_{\text{int}} \omega^2 / c^2$ ,  $s$  is the surface of the scatterer, and  $\Psi_n(k\mathbf{r})$  is substituted by  $\text{Re } \Psi_n(k\mathbf{r})$  wherever  $\text{Re } \mathbf{Q}$  appears. In our case  $\epsilon_{\text{ext}} = 1$  (vacuum) and  $\epsilon_{\text{int}}$  is the corresponding value for silver.

Equation (5) permits the calculation of the internal field, at least when  $|\mathbf{r}| < r_{\min}$ . Eliminating  $\mathbf{G}$  from Eqs. (4) and (5), we obtain a relation between the coefficients of the scattered and incident fields:

$$\mathbf{F} = \underline{\mathbf{T}} \mathbf{A}, \quad (7)$$

where  $\underline{T}$  is the T matrix of the single scatterer defined as

$$\underline{T} = -\underline{Q}^{-1} \text{Re } \underline{Q}. \quad (8)$$

With Eq. (2) the local fields can be calculated for  $|\mathbf{r}| < r_{\min}$  by using the  $\underline{Q}$  matrix and for  $|\mathbf{r}| > r_{\max}$  by using the T matrix, but the region  $r_{\max} > |\mathbf{r}| > r_{\min}$  is forbidden because the convergence of the expansions of Eq. (2) is not ensured. Some research has been done to improve on this shortcoming; Bringi and Seliga<sup>17</sup> proposed a mathematical procedure that used the T-matrix framework to calculate fields inside this forbidden zone. Barber *et al.*<sup>18</sup> used a method based on the T-matrix approach to evaluate local fields not only at the tips but at any place on the surface of the spheroids.

### b. Rotation of the T Matrix

For the rotation of the T matrix, two coinciding coordinate systems are considered. With respect to the origin of both systems, the Euler angles  $\alpha$ ,  $\beta$ , and  $\gamma$  are used to rotate one of the systems relative to the other.<sup>19</sup> The rotation of the basis functions is accomplished by transforming the spherical harmonics under finite rotations. These transformation properties are given in the quantum mechanics literature (e.g., Ref. 20).

Explicitly, if  $\Psi_{nm\sigma}$  and  $\Psi_{nm'\sigma}$  are the vector spherical functions in the rotated and nonrotated coordinate systems, respectively, then one can write

$$\Psi_{nm\sigma} = \sum_{m'\nu} D_{m'\nu, m\sigma}(\alpha, \beta, \gamma) \Psi_{nm'\sigma},$$

where the index  $n$  is invariant under rotations and the rotation matrix  $\underline{D}$  is a function of the Euler angles that define the relative orientation of the two coordinate system.<sup>20</sup>

The incident and scattered electric fields in Eq. (2) are then expanded with respect to the two coordinate systems. A relationship between the expansion coefficients for  $\epsilon_0$  and  $\epsilon_s$  in the two systems can be established by using the orthogonality of the vector spherical functions. Using the definition of the T matrix, we finally obtain

$$\underline{T}' = \underline{D}^{-1}(\alpha, \beta, \gamma) \underline{T} \underline{D}(\alpha, \beta, \gamma), \quad (9)$$

where  $\underline{T}'$  is the T matrix for the rotated coordinate system.

### C. Clusters

The T-matrix formalism has been extended to systems with more than one scatterer by Peterson and Ström<sup>9</sup> by using the translation theorems for the vector spherical functions.<sup>21</sup> The translation properties of  $\Psi_n$  and  $\text{Re } \Psi_n$  are summarized by Ref. 22:

$$\begin{aligned} \text{Re } \Psi_n(\mathbf{r} + \mathbf{a}) &= \sum_{\tau'n'} R_{m,\tau'n'}(\mathbf{a}) \text{Re } \Psi_{\tau'n'}(\mathbf{r}), \\ \Psi_n(\mathbf{r} + \mathbf{a}) &= \sum_{\tau'n'} \sigma_{m,\tau'n'}(\mathbf{a}) \Psi_{\tau'n'}(\mathbf{r}), \quad |\mathbf{a}| > |\mathbf{r}|, \\ \Psi_n(\mathbf{r} + \mathbf{a}) &= \sum_{\tau'n'} R_{m,\tau'n'}(\mathbf{a}) \Psi_{\tau'n'}(\mathbf{r}), \quad |\mathbf{a}| < |\mathbf{r}|, \end{aligned}$$

where  $\sigma_{m,\tau'n'}$  and  $R_{m,\tau'n'}$  are the elements of the translation matrices as defined in Ref. 9.

Peterson and Ström obtained a T matrix for the cluster of two particles in terms of the T matrices of each single scatterer,

$$\begin{aligned} \underline{T}(1, 2) &= \underline{R}(\mathbf{a}_1) \{ \underline{T}(1) [ \underline{1} - \underline{\sigma}(-\mathbf{a}_1 + \mathbf{a}_2) \\ &\quad \times \underline{T}(2) \underline{\sigma}(-\mathbf{a}_2 + \mathbf{a}_1) \underline{T}(1) ]^{-1} \\ &\quad \times [ \underline{1} + \underline{\sigma}(-\mathbf{a}_1 + \mathbf{a}_2) \underline{T}(2) \underline{R}(\mathbf{a}_1 - \mathbf{a}_2) ] \} \\ &\quad \times \underline{R}(-\mathbf{a}_1) + \underline{R}(\mathbf{a}_2) \{ \underline{T}(2) [ \underline{1} - \underline{\sigma}(-\mathbf{a}_2 + \mathbf{a}_1) \\ &\quad \times \underline{T}(1) \underline{\sigma}(-\mathbf{a}_1 + \mathbf{a}_2) \underline{T}(2) ]^{-1} [ \underline{1} + \underline{\sigma}(-\mathbf{a}_2 + \mathbf{a}_1) \\ &\quad \times \underline{T}(1) \underline{R}(\mathbf{a}_2 - \mathbf{a}_1) ] \} \underline{R}(-\mathbf{a}_2), \quad (10) \end{aligned}$$

where  $\mathbf{a}_1$  and  $\mathbf{a}_2$  are the distances from the origin to the center of scatterers 1 and 2, respectively.

The scattered field can be expressed in terms of the incident field by using the T-matrix with the following relationship:

$$\epsilon_s = \underline{T} \epsilon_0.$$

Most of the results presented herein will be expressed in terms of the total electric field given by

$$\epsilon_t = \epsilon_s + \epsilon_0. \quad (11)$$

It is important to remember that the local fields can only be calculated by starting from a minimum circumscribing sphere around the scatterers to ensure convergence of the spherical wave expansions.

With these two transformations, rotation and translation, it is then possible to consider clusters with variables separation and arbitrary orientation of the constituent metallic spheroids.

### 3. Discussion

The quantities discussed here are the normalized local field intensities  $|\epsilon_t/\epsilon_0|^2$  in the neighborhood of the clusters of two prolate spheroids. These have been calculated by inserting the individual T matrices of each spheroid, Eq. (8), into Eq. (10), thus yielding the effective T matrix for the cluster as a function of interparticle distance. In the case of a different orientation between the spheroids, their rotation has been taken into account by applying Eq. (9) and substituting the rotated T matrix into Eq. (10). Finally, the total electric field vector has been calculated from Eq. (11), from which the enhancement of the intensity of the field was obtained by taking the square of the magnitude of that vector.

To illustrate the general results from this type of calculation, we use two identical prolate spheroids with an aspect ratio  $a/b = 0.9$  and  $a = 5$  nm, where  $a$  and  $b$  are the semiminor and semimajor axes of the prolate spheroid, respectively. The formalism permits the treatment of spheroids of any eccentricity, but because of computational time and memory limitations only the described size is considered. Although the clusters of spheroids used here are in the long-wavelength regime, the calculations are elec-

hydrodynamic in nature because the formalism is developed from the vector Helmholtz Eq. (1); results can and have been obtained for other sizes and aspect ratios.<sup>14</sup>

The calculations were done by taking the direction of propagation of the incident wave front to be along the  $y$  axis. The polarization of the electric field is parallel to the direction of the interparticle distance, which is the  $x$  axis. By testing other directions of incidence and polarizations, we have determined that the latter orientation gives the highest scattered-intensity enhancement (of the order of  $10^3$ ) for the configuration of the clusters considered; we therefore choose these as our working parameters. The calculations of the electric field are performed as a function of interparticle separation and relative orientation of the spheroids.

Two resonant peaks are exhibited by the spectra of all the geometrical configurations considered. It is worth noting that this behavior is due to the interparticle multipolar interactions, because only one peak is observed when the spheroids are sufficiently far apart (when  $d$ , the interparticle distance, is of the order of  $4b$ ).

The two resonant peaks experience a characteristic red shift as a function of decreasing distance between spheroids for all the clusters considered. This shift reflects the interaction among the spheroids in the cluster, which becomes stronger as the distance between the centers of the particles decreases, thereby resulting in maximum shift for touching spheroids. Figure 1 shows the calculated spectrum for the cluster of two spheroids whose semimajor axes are aligned with the incident electric field. Because this is the more elongated cluster, it exhibits the highest enhancement shown in this paper (of the order of  $10^3$ ). The closer the spheroids the higher the interac-

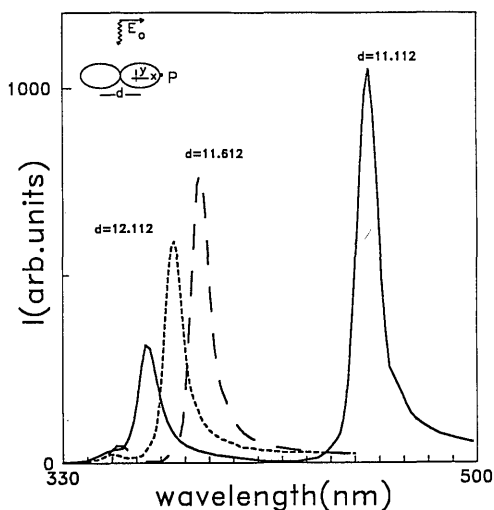


Fig. 1. Intensity of the total electric field at the point of observation P as a function of wavelength for a cluster of aligned spheroids with  $a/b = 0.9$  and  $a = 5$  nm for three interparticle distances ( $d = 11.112$  nm  $= 2b$ , touching spheroids, 11.612 nm, and 12.112 nm). The direction of the incident radiation is along the  $y$  axis and the polarization is parallel to the  $x$  axis.

tion between them and the more multipolar terms are required in the calculation. As the interparticle distance decreases, the low-energy peak shifts more rapidly toward the red than the high-energy peak. This behavior is related to higher multipolar terms, other than the dipolar, which become more important as the spheroidal constituents of the cluster approach each other. As the interparticle distance diminishes, the low-energy peak decreases rapidly in energy while its intensity increases. The high-energy peak disappears when  $d \approx 3b$ , the decoupling distance, whereas the low-energy peak shifts to the resonant wavelength corresponding to the isolated particle.

The effect of rotation has been analyzed by rotating only one spheroid and by examining the local field at opposite points on the exclusion sphere on the axis that joins the centers of the particles, because for this case the cluster is asymmetric. The analysis is also performed by rotating both spheroids, thus maintaining the mirror symmetry of the cluster. In both cases the interparticle distance is held constant. Figures 2(a) and 2(b) show the behavior of the local field observed at the two previously indicated points on the  $x$  axis when only one spheroid is rotated. Figure 2(a) describes the field near the nonrotated spheroid and Fig. 2(b) describes that near the rotated spheroid. The difference between the two observation points is in the intensity of the local field, whereas the position of the resonance peaks remains constant. This constance is to be expected because the resonant peaks are phenomena associated with surface plasmons of the cluster that depend on the configuration of the whole cluster and not on the point of observation. Figure 3 shows the spectrum of the simultaneously rotated spheroids. The configuration  $\theta = 90^\circ$  coincides with the cluster of Fig. 1, which exhibits the highest enhancement in this paper. The rotation of the spheroids does not affect the number of peaks observed in the spectrum, although their energies are shifted toward the red as a function of increasing angle measured with respect to the  $y$  axis. For this case the red shift of the peaks is also attributed to the increase in interaction between the spheroids, because for an isolated spheroid the shift in energy as a function of angle of rotation is negligible for slightly eccentric spheroids. The maximum enhancement is obtained in Figs. 2(a) and 2(b) when the rotated spheroid is at an angle of  $\theta = 90^\circ$ . This occurrence is reasonable because the semimajor axis of the rotated spheroid is perpendicular to the polarization of the incident electric field at  $\theta = 0^\circ$  and is parallel at  $\theta = 90^\circ$ , thereby enhancing the field by its geometry and directing the energy more efficiently toward the other radiating spheroid. As we expected, the largest red shift and enhancement occurs in Fig. 3 where both spheroids are simultaneously rotated.

The resonant wavelengths for the cases shown in Figs. 1 and 3 have been studied as functions of interparticle distance  $d$  and orientation  $\theta$ , respectively. Figures 4(a) and 4(b) display the behavior of the

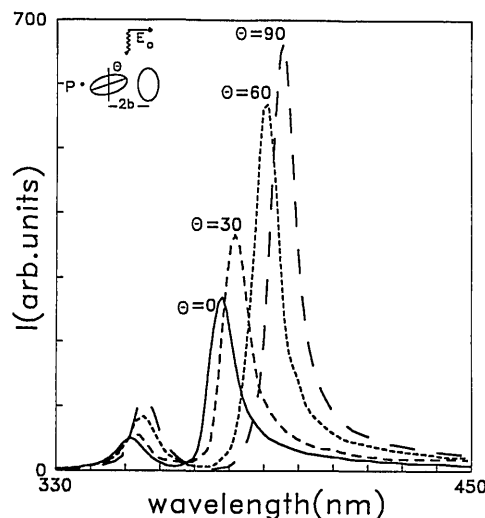
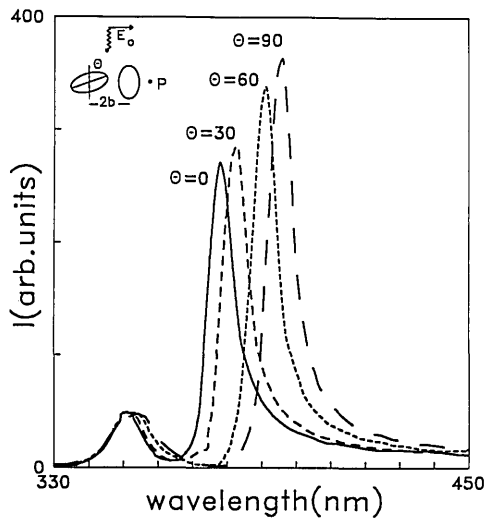


Fig. 2. (a), (b) Intensity of the total electric field at the point P as a function of wavelength for a cluster of spheroids with  $a/b = 0.9$  and  $a = 5$  nm for different angles of orientation of the spheroids with respect to the vertical axis. The directions of the incident radiation and the polarization are as shown.

low-energy peaks as a function of orientation angle and of interparticle separation. Figures 5(a) and 5(b) provide this same analysis for the high-energy peak. A least-squares fit to the data was made for all four cases to determine the behavior of the red shifts as a function of interparticle separation and also as a function of orientation. The spread of calculated resonance wavelengths about the smooth curves is due to the fact that all resonant wavelengths analyzed in Figs. 4 and 5 were obtained from a spline interpolation of the calculated cluster spectra. The uncertainty introduced by this interpolation in determining the resonant wavelengths is of the order of  $\pm 2$  nm.

In the case of both the low- and high-energy peaks for the rotated spheroids, the shift toward the red shows a sinusoidal behavior, as is illustrated in Figs. 4(a) and 5(a). A least-squares fit of this data gives a functional behavior for the shift that is governed by

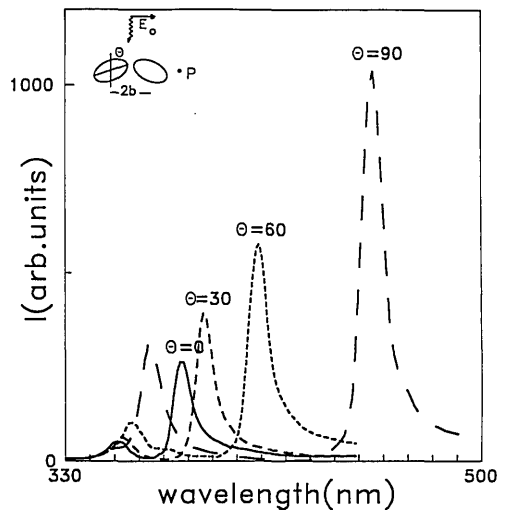


Fig. 3. Intensity of the total electric field at the point P as a function of wavelength for a cluster of simultaneously rotated spheroids with  $a/b = 0.9$ ,  $a = 5$  nm for different angles of rotation of the two spheroids. The directions of the incident radiation and the polarization are as shown.

the simple relationship  $\lambda(\theta) = A + B \sin^2(\theta)$ . For Fig. 4(a),  $A = 376.7$  nm and  $B = 47.8$  nm; for Fig. 5(a),  $A = 351.8$  nm and  $B = 7.2$  nm.

From Figs. 4(b) and 5(b), it appears that the position of the peaks have an exponential behavior as a function of increasing interparticle distance. A curve fitting gives the functional relationship  $\lambda(d) = \lambda' + \delta\lambda \exp[-(d - d_0)/\eta]$ . For the case of the low-energy peak,  $\lambda'$  was taken to be the resonant wavelength for the decoupled cluster, i.e., the resonant frequency of an isolated spheroid. Here  $\delta\lambda$  is the difference between the resonant wavelength of the touching spheroids and the resonant wavelength with no coupling and  $d_0$  is the touching distance  $2b$ . The

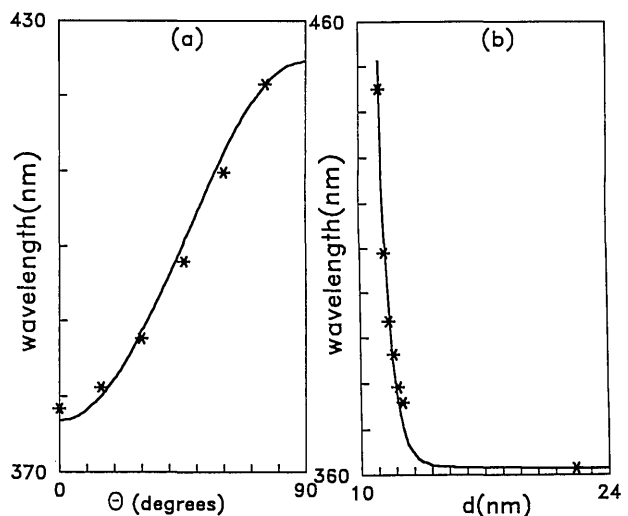


Fig. 4. Shift in the resonant wavelength for the low-energy peak as a function of (a) the rotation angle  $\theta$  of the simultaneously rotated spheroids, and (b) interparticle separation  $d$  for the aligned spheroids. The solid curve represents a least-squares fit to the calculated points.

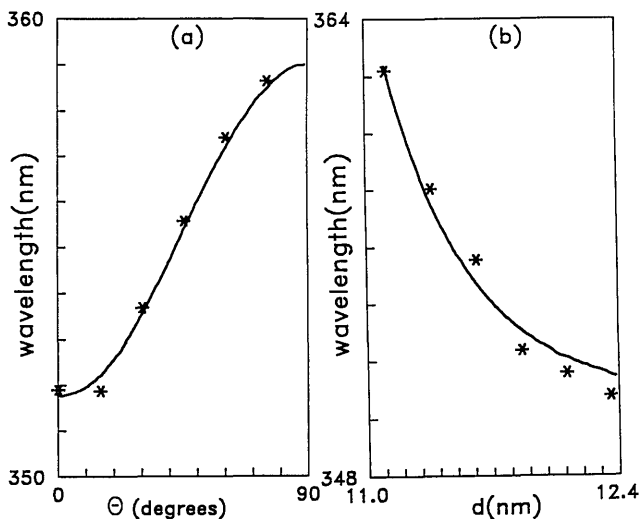


Fig. 5. Shift in the resonant wavelength for the high-energy peak as a function of (a) the rotation angle  $\theta$  of the simultaneously rotated spheroids, and (b) interparticle separation  $d$  for the aligned spheroids. The solid curve represents a least squares fit to the calculated points.

only fitting parameter used is  $\eta$ , which corresponds to a decay factor. For Fig. 4(b),  $\lambda' = 361.5$  nm,  $\delta\lambda = 94$  nm, and the fitted parameter is  $\eta = 0.57$  nm. For the case of the high-energy peak it is also necessary to fit  $\lambda'$ ; the resulting fitted curve for Fig. 5(b) yields  $\lambda' = 350$  nm,  $\delta\lambda = 13.6$  nm, and  $\eta = 0.32$  nm. From the analysis it is evident that the low-energy peak suffers a considerably larger shift in wavelength than the high-energy peak as a function of both angle and interparticle distance.

The decoupling distance for the cases discussed here occur at  $d \approx 3b$ . For all other cases studied by us the decoupling distance has been found to be  $d \approx 4b$ , which is twice the distance of touching spheroids.

#### 4. Conclusions

A T-matrix formalism has been used to calculate the local electric field near clusters of metallic spheroids, and the influence of clustering on their spectrum has been investigated as a function of interparticle distance  $d$  and relative orientation  $\theta$  in the long-wavelength regime. The calculations show two resonant peaks in the spectrum caused by interparticle interactions, which is in contrast with one peak in the spectrum of the single spheroid. The high-energy peak disappears and the low-energy peak becomes the peak of the isolated spheroid for interparticle distances of  $4b$ . This fact should prove useful in the analysis of clusters of more than two ellipsoidal particles.

As a result of the interaction among the spheroids that form the cluster, enhancements of up to  $10^3$  are observed. Higher enhancements should be observed for more eccentric ellipsoidal constituents of the cluster. The enhancement is shown to be sensitive to the relative orientation of the spheroids and the interparticle distance. Both resonant peaks are red shifted as a function of reduced interparticle distance

and of increasing angle of rotation with respect to the  $y$  axis.

The position of the higher-energy peak is less sensitive to interparticle distance than the lower-energy one, and rotations are less effective in shifting the peaks than the separation of the spheroids. Through a least-squares fit, we demonstrated that the shifting of the low-energy peak obeys an exponential relationship as a function of the varying interparticle distance that decays to the value of an isolated spheroid for values of  $d \approx 3b$ , whereas the red shift obeys a sinusoidal relationship as a function of the angle of rotation of the spheroids.

For experimental systems composed of a collection of scatterers with a random distribution of interparticle distances and orientations, these calculations will be important in predicting the estimated effective width of the observed resonances. The predicted width is expected to be greater than the ones shown here because such a system will have contributions from clusters with a wide variety of interparticle distances and relative orientations. A rough estimate suggests that the resonant peak of that system should have a width of the same order as the difference between the resonant energy of the cluster of touching spheroids and the resonant energy of a decoupled cluster.

Recently some efforts have appeared in the literature that treat clusters of spheroids by using ellipsoidal harmonics,<sup>23</sup> but to our knowledge only calculations restricted to the far zone have been performed. We do not expect that the use of ellipsoidal harmonics will simplify in any significant manner the calculation of the field in the near zone, because a cluster does not have either spherical or ellipsoidal symmetry; therefore, we do not anticipate any advantage of one expansion over the other.

This research was partially supported by the National Science Foundation grant INT-8509185 and by the U. S. Army Research Office grant DAAL03-89-G-0114.

#### References

1. Lord Rayleigh, "The incidence of light upon a transparent sphere of dimensions comparable with the wave-length," *Proc. R. Soc. London Ser. A* **84**, 25-46 (1910).
2. G. Mie, "Beiträge zur optik trüber medien, speziell kolloidaler metallösungen," *Ann. Phys. (Leipzig)* **25**, 377-445 (1908).
3. R. P. Devatty and A. J. Sievers, "Single-particle collective-mode coupling and the Mie resonance in small metallic particles: optical properties of colloidal Na in NaCl," *Phys. Rev. B* **24**, 1079-1082 (1981).
4. J. M. Calleja and F. Agullo-Lopez, "Photoconductivity of potassium colloids in KCl single crystals," *J. Phys. Chem. Solids* **37**, 363-367 (1976).
5. E. Rzepka, L. Taurel, and S. Lefrant, "First-order Raman scattering induced by Na and Ag colloids in NaCl, NaBr and NaI," *Surf. Sci.* **106**, 345-349 (1981).
6. M. Moskovits, "Surface-enhanced spectroscopy," *Rev. Mod. Phys.* **57**, 783-826 (1985).
7. H. Reimer and F. Fischer, "SERS from Ag colloids in alkali halide crystals," *Phys. Status Solidi B* **124**, 61-67 (1984).

8. W. Kleeman, "Absorption of colloidal silver in KCl," *Z. Phys.* **215**, 113–120 (1968).
9. B. Peterson and S. Ström, "T-matrix for electromagnetic scattering from an arbitrary number of scatters and representations of  $E(3)$ ," *Phys. Rev. D* **8**, 3661–3678 (1973).
10. F. Claro, "Theory of resonant modes in particulate matter," *Phys. Rev. B* **30**, 4989–4999 (1984).
11. R. Fuchs and F. Claro, "Multipolar response of small metallic spheres: nonlocal theory," *Phys. Rev. B* **35**, 3722–3727 (1987).
12. Z. Chen, P. Sheng, D. A. Weitz, H. M. Lindsay, M. Y. Lin, and P. Meakin, "Optical properties of aggregate clusters," *Phys. Rev. B* **37**, 5232–5235 (1988).
13. N. Liver, A. Nitzan, and J. I. Gersten, "Local fields in cavity sites of rough dielectric surfaces," *Chem. Phys. Lett.* **111**, 449–453 (1984); N. Liver, A. Nitzan, and K. F. Freed, "Radiative and nonradiative decay rates of molecules absorbed on clusters of small dielectric particles," *J. Chem. Phys.* **82**, 3831–3840 (1985).
14. L. Cruz, L. Fonseca, and M. Gomez, "T-matrix approach for the calculation of local fields in the neighborhood of small clusters in the electrodynamic regime," *Phys. Rev. B* **40**, 7491–7500 (1989).
15. P. B. Johnson and R. W. Christy, "Optical constants of noble metals," *Phys. Rev. B* **6**, 4370–4379 (1972).
16. P. C. Waterman, "Symmetry, unitarity, and geometry in electromagnetic scattering," *Phys. Rev. D* **3**, 835–839 (1971).
17. V. N. Bringi and T. A. Seliga, "Surface currents and 'near' zone fields," in *Acoustic, Electromagnetic and Elastic Wave Scattering—Focus on the T-Matrix Approach*, V. K. Varadan and V. V. Varadan, eds. (Pergamon, New York, 1979), pp. 79–90.
18. P. W. Barber, R. K. Chang, and H. Massoudi, "Electrodynamic calculations of the surface-enhanced electric intensities on large Ag spheroids," *Phys. Rev. B* **27**, 7251–7260 (1983).
19. G. Arfken, *Mathematical Methods for Physicists* (Academic, New York, 1985), p. 198.
20. A. R. Edmonds, *Angular Momentum in Quantum Mechanics* (Princeton U. Press, Princeton, N.J., 1957).
21. O. R. Cruzan, "Translational addition theorems for spherical vector wave functions," *Q. Appl. Math.* **20**, 33–40 (1962).
22. V. K. Varadan, "Elastic wave scattering," in *Acoustic, Electromagnetic and Elastic Wave Scattering—Focus on the T-Matrix Approach*, V. K. Varadan and V. V. Varadan, eds. (Pergamon, New York, 1979), pp. 33–59.
23. M. F. R. Cooray and I. R. Ciric, "Electromagnetic wave scattering by a system of two spheroids of arbitrary orientation," *IEEE Trans. on Antennas and Propag.* **37**, 608–618 (1989).